BIOCHEMISTRY
including biophysical chemistry & molecular biology

Article

pubs.acs.org/biochemistry

The Dimanganese(II) Site of *Bacillus subtilis* Class Ib Ribonucleotide Reductase

Amie K. Boal,[†] Joseph A. Cotruvo, Jr.,[‡] JoAnne Stubbe,*[,‡,§] and Amy C. Rosenzweig*[,†]

[†]Departments of Molecular Biosciences and Chemistry, Northwestern University, Evanston, Illinois 60208, United States

[‡]Department of Chemistry and [§]Department of Biology, Massachusetts Institute of Technology, Cambridge, Massachusetts 02139, United States

Supporting Information

ABSTRACT: Class Ib ribonucleotide reductases (RNRs) use a dimanganese-tyrosyl radical cofactor, Mn^{III}_2-$Y^{\bullet}$, in their homodimeric NrdF (β2) subunit to initiate reduction of ribonucleotides to deoxyribonucleotides. The structure of the Mn^{II}_2 form of NrdF is an important component in understanding O_2-mediated formation of the active metallocofactor, a subject of much interest because a unique flavodoxin, NrdI, is required for cofactor assembly. Biochemical studies and sequence alignments suggest that NrdF and NrdI proteins diverge into three phylogenetically distinct groups. The only crystal structure to date of a NrdF with a fully ordered and occupied dimanganese site is that of *Escherichia coli* Mn^{II}_2-NrdF, prototypical of the enzymes from actinobacteria and proteobacteria. Here we report the 1.9 Å resolution crystal structure of *Bacillus subtilis* Mn^{II}_2-NrdF, representative of the enzymes from a second group, from *Bacillus* and *Staphylococcus*. The structures of the metal clusters in the β2 dimer are distinct from those observed in *E. coli* Mn^{II}_2-NrdF. These differences illustrate the key role that solvent molecules and protein residues in the second coordination sphere of the Mn^{II}_2 cluster play in determining conformations of carboxylate residues at the metal sites and demonstrate that diverse coordination geometries are capable of serving as starting points for Mn^{III}_2-$Y^{\bullet}$ cofactor assembly in class Ib RNRs.

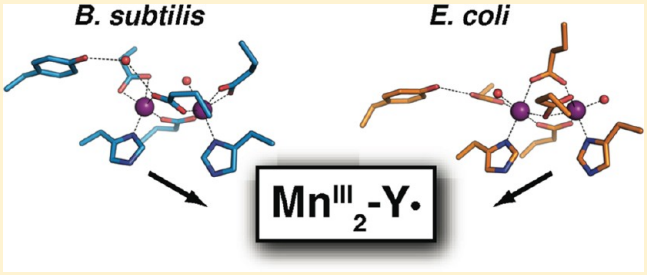

Ribonucleotide reductases (RNRs) catalyze the reduction of all four nucleotides to their corresponding deoxynucleotides, providing the precursors necessary for DNA synthesis and repair in all organisms.[1] All class I RNRs initiate nucleotide reduction by the reversible oxidation of a cysteine residue to a thiyl radical in their α2 subunits by unique dinuclear metal cofactors that reside 35 Å away in their β2 subunits.[2] Three subclasses of the class I enzymes are now recognized: Ia, Ib, and Ic.[3] In all three subclasses, the dinuclear clusters are ligated by two histidines and four carboxylate ligands within a four-helix bundle.[4,5] The class Ia RNRs are found in eukaryotes and a few prokaryotes, with the enzyme from *Escherichia coli* serving as a prototype. Their essential diferric-tyrosyl radical (Fe^{III}_2-$Y^{\bullet}$) cofactor is formed in vitro by self-assembly from a diferrous (Fe^{II}_2) site in the β2 subunit (NrdB) upon reaction with O_2 and a reductant.[6] Thus far, only the class Ic RNR from the intracellular pathogen *Chlamydia trachomatis* has been characterized. In vitro, its β2 subunit can be loaded with a $Mn^{II}Fe^{II}$ cluster that reacts with O_2[7] or H_2O_2[8] to form an active $Mn^{IV}Fe^{III}$ cofactor.

The class Ib RNRs, found in many eubacteria, including a number of important human pathogens,[9,10] have the same ligand set as the class Ia enzymes but are unique in that they can assemble both active Fe^{III}_2-$Y^{\bullet}$ and active dimanganese(III)-$Y^{\bullet}$ (Mn^{III}_2-$Y^{\bullet}$) cofactors in their β2 (NrdF) subunits. The Fe^{III}_2-$Y^{\bullet}$ cofactor can be self-assembled in vitro,[11,12] similar to the class Ia enzymes. The Mn^{III}_2-$Y^{\bullet}$ cofactor can be generated in vitro by oxidation of a dimanganese(II) site (Mn^{II}_2), using the flavodoxin-like protein NrdI[13] and O_2. The same manganese cofactor has recently been identified in vivo in *Corynebacterium ammoniagenes*,[14,15] *E. coli*,[16,17] and *Bacillus subtilis*.[18] Our studies with the *E. coli* (*Ec*) and *B. subtilis* (*Bs*) NrdF proteins have shown that an active cofactor can be formed only when Mn^{II}_2-NrdF is incubated with the reduced (hydroquinone, hq) form of NrdI[19,20] and O_2; exogenous oxidants are nonfunctional.[12,13] Biochemical[13] and structural[21] studies have further suggested that O_2 is reduced to either HOO(H) or $O_2^{\bullet-}$ by NrdI in complex with NrdF, and the oxidant is then channeled directly to Mn2 of the Mn^{II}_2-NrdF center (see Figure 1 for metal site designations).

How the class Ib RNRs can assemble active Fe^{III}_2-$Y^{\bullet}$ and Mn^{III}_2-$Y^{\bullet}$ cofactors from their reduced states using identical metal binding motifs and different oxidants is an important question raised by these observations. To understand the subtle differences that dictate specific metal loading and reactivity with different oxidants, high-resolution structures of protein in the reduced and oxidized forms are essential. A number of Fe^{II}_2-NrdF and NrdB structures have been obtained by soaking

Received: December 26, 2011
Revised: March 20, 2012
Published: March 23, 2012

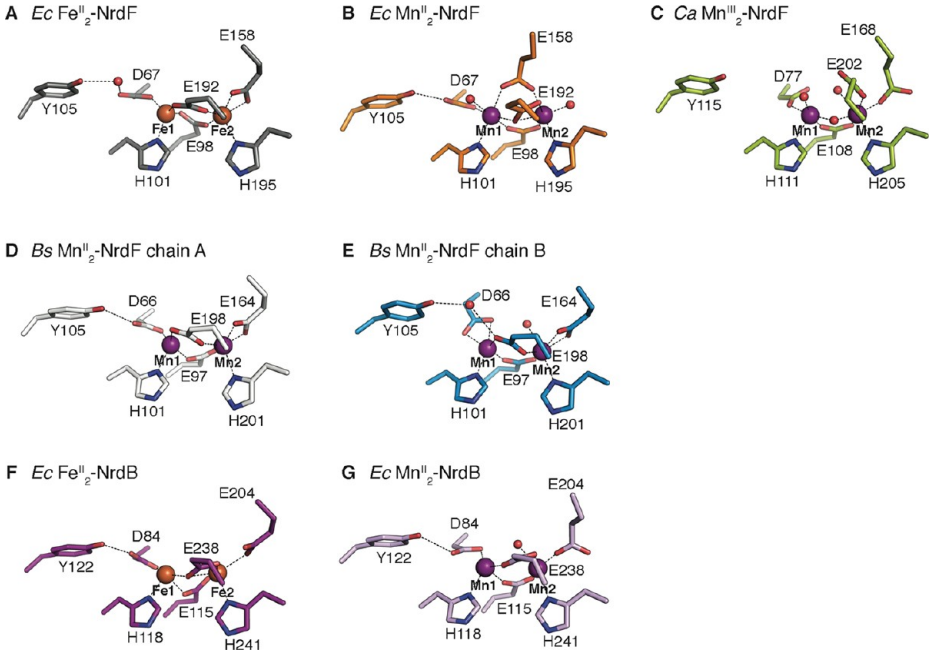

Figure 1. Stick representations of the active site in class Ib β2 structures for (A) *Ec* Fe$^{II}_2$-NrdF (PDB entry 3N38), (B) *Ec* Mn$^{II}_2$-NrdF (PDB entry 3N37), (C) *Ca* Mn$^{III}_2$-NrdF (PDB entry 3MJO), and (D) *Bs* Mn$^{II}_2$-NrdF chain A and (E) chain B. Class Ia structures for *Ec* Fe$^{II}_2$-NrdB (F) (PDB entry 1PIY) and Mn$^{II}_2$-NrdB (G) (PDB entry 1MRR) are shown in comparison.

crystals of apoprotein with Fe^{II} [21−24] (Figure 1A,F) or by chemical reduction or photoreduction of crystals containing the Fe$^{III}_2$ cluster.[25−27] Not all of these structures have fully occupied Fe$^{II}_2$ clusters, however. For instance, the *Ec* Fe$^{II}_2$-NrdF structure obtained by Fe^{II} soaking is only 50% occupied at each metal site,[21] whereas the *Ec* Fe$^{II}_2$-NrdB structure obtained by the same method is fully occupied.[23] At present, only the structure of *Ec* Mn$^{II}_2$-NrdF[21] has been obtained by cocrystallization with metal, revealing fully occupied Mn$^{II}_2$ sites. Each Mn^{II} ion is six-coordinate, including one solvent ligand (Figure 1B). Unusual features of this structure and its complex with oxidized NrdI (NrdI$_{ox}$) and NrdI$_{hq}$ are that Glu 158 (*Ec* numbering) bridges both metals in μ-1,3 fashion and that the water molecule associated with Mn2 occupies a unique terminal site. In all other ferritin superfamily proteins,[28] the corresponding Glu coordinates to metal site 2 alone, occupying the site of the unique Mn2 water ligand in the *Ec* structure (Figure 1). Interestingly, the Mn2 water ligand is hydrogen bonded to other ordered waters in a hydrophilic channel proposed to facilitate delivery of the oxidant from NrdI, suggesting that dissociation of this water molecule, which may involve conformational change(s) in carboxylate ligands, must precede oxidant binding.[21] The importance of carboxylate shifts[29] during cofactor assembly is underscored by comparison of the *Ec* structures with a high-resolution structure of the oxidized, Mn$^{III}_2$ form of *C. ammoniagenes* (*Ca*) NrdF (Figure 1C), with the cofactor assembled in vivo.[14] The NrdFs from *E. coli* and *C. ammoniagenes* are highly identical in sequence (66%) with all residues within 7 Å of the metal site completely conserved. In the *Ca* Mn$^{III}_2$-NrdF structure, three of the four carboxylate ligands adopt distinct conformations relative to their counterparts in *Ec* Mn$^{II}_2$-NrdF (Figure 1B,C).

As part of a comprehensive approach to understand in molecular detail the mechanism of Mn$^{III}_2$-Y$^{\bullet}$ cofactor assembly, the crystal structure of the Mn$^{II}_2$ form of *Bs* NrdF has been determined to 1.9 Å resolution. *Bs* NrdF was chosen for study because it has the highest Mn$^{III}_2$-Y$^{\bullet}$ content (0.6 Y$^{\bullet}$/β2) generated to date[18] and belongs to the Bacillales group of class Ib enzymes, for which no structural data were available. The Mn$^{II}_2$ sites in each monomer of the NrdF dimer display slightly different coordination environments (Figure 1D,E), each similar to but distinct from those in previously determined structures of the Mn$^{II}_2$ and Fe$^{II}_2$ forms of *Ec* class Ia NrdB and class Ib NrdF.[21,23−26] This structure of *Bs* Mn$^{II}_2$-NrdF highlights the important role of second-coordination sphere water molecules in controlling the conformation of carboxylate metal ligands. In addition, it suggests how coordination chemistry differences between manganese and iron impact metal site structure. Finally, viewed in the context of the differences in sequence and biochemistry between the *Ec* and *Bs* groups of class Ib RNRs, the *Bs* NrdF structure and a model of the putative *Bs* NrdI-NrdF complex provide insight into potential similarities and differences in the nature of the NrdI interface and the mechanism of Mn$^{II}_2$ cofactor activation among these NrdFs.

MATERIALS AND METHODS

Purification of *B. subtilis* Apo NrdF. The NrdF construct[18] contains an N-terminal His$_6$ tag and linker, MH$_6$SSGLVPRGSH, preceding the N-terminal Met of the wild-type protein. The tag was not removed prior to crystallization. Apo NrdF was purified as described previously,[18] but an additional anion exchange column was necessary to obtain crystals. Apo NrdF (500 μL, 450 μM dimer) purified by Ni-NTA column chromatography was loaded onto a Pharmacia Mono Q column (HR 16/10, 20 mL column volume, 1 mL/min flow rate) preequilibrated in 50 mM HEPES, 5% glycerol, and 200 mM NaCl, pH 7.6. The column was washed with 15 mL of the same buffer at a rate of 1 mL/min, and the protein was eluted with a 120 mL linear gradient from 200 to 800 mM NaCl in the same buffer (1 mL/min), collecting 2 min fractions. The fractions containing the major protein peak

Table 1. Data Collection and Refinement Statistics

	Bs NrdF	*Bs* NrdF (Mn ano)	*Bs* NrdF 15 equiv (Mn ano)
Data Collection			
wavelength (Å)	1.078	1.856	1.856
space group	$P2_12_12$	$P2_12_12$	$P2_12_12$
cell dimensions			
a, *b*, *c* (Å)	110.525, 112.912, 51.286	111.246, 112.889, 52.810	110.528, 113.090, 51.362
resolution (Å)	50.00−1.90 (1.93−1.90)	50.00−2.42 (2.46−2.42)	50.00−2.13 (2.17−2.13)
R_{sym} or R_{merge}	0.100 (0.615)	0.155 (0.573)	0.130 (0.516)
$I/\sigma I$	18.5 (2.5)	23.9 (4.6)	26.7 (2.2)
completeness (%)	96.5 (80.4)	100 (99.7)	98.0 (78.9)
redundancy	6.9 (5.6)	12.0 (7.3)	11.1 (3.0)
Refinement			
resolution (Å)	50.00−1.90		
no. of reflections	46879		
R_{work}/R_{free}	0.1857/0.2240		
no. of atoms			
protein	4786		
Mn^{II}	4		
other ion/ligand	2		
water	294		
B factor			
protein	26.3		
Mn^{II}	24.7		
other ion/ligand	50.2		
water	33.6		
root-mean-square deviation			
bond lengths (Å)	0.009		
bond angles (deg)	1.089		

eluted at 350−400 mM NaCl and were pooled, concentrated, and exchanged into 50 mM HEPES, 5% glycerol, pH 7.6 by repeated concentration and dilution using an Amicon Ultra YM30 centrifugal concentrator.

***B. subtilis* Mn^{II}_2-NrdF Structure.** Apo NrdF [36 mg/mL in 50 mM HEPES, 5% glycerol, pH 7.6] was incubated with 4 equiv of $MnCl_2$ per β2 for 20 min on ice prior to the crystal drop setup. Additional data sets were collected on crystals grown with 15 equiv of $MnCl_2$. Single rectangular prism-shaped crystals were obtained using the hanging drop vapor diffusion method at room temperature with 25% (w/v) PEG 4000, 0.375 M lithium sulfate, and 0.1 M HEPES, pH 6.5. Crystals were briefly soaked in a cryoprotectant solution [35% (w/v) PEG 4000, 0.1 M lithium sulfate, 0.1 M HEPES, pH 6.5], mounted in rayon loops, and flash-frozen in liquid nitrogen.

All crystallographic data sets were collected at the Life Sciences Collaborative Access Team (LS-CAT) and the National Institute of General Medical Sciences and National Cancer Institute Collaborative Access Team (GM/CA-CAT) beamlines at the Advanced Photon Source. Data sets were processed using the HKL2000 package.[30] The structure was determined by molecular replacement using PHASER[31] with the coordinates of *Ec* Mn^{II}_2-NrdF (PDB entry 3N37) as the initial model. Model building and refinement were performed with Coot[32] and Refmac5,[33] respectively. The data collection and refinement statistics are listed in Table 1. The final model consists of residues 1−290 of 329 in chain A (residues 4−9 are partially disordered), residues 3−293 in chain B, four Mn^{II} ions, two sulfate molecules, and 294 water molecules. Electron density was not observed for the N-terminal tag and linker or the final 33−36 residues at the C-terminus of the protein, as in all other β2 structures. Ramachandran plots calculated with PROCHECK[34] and Molprobity[35] indicate that 99.9% of the residues are in the allowed and additionally allowed regions. All figures were prepared with PyMOL.[36] Anomalous difference Fourier maps calculated using data collected at the Mn absorption edge on a second crystal [*Bs* NrdF (Mn ano) (Table 1)] reveal strong density at both NrdF active sites. Differences in Mn peak intensity are observed between the active sites in β2 such that the Mn^{II} sites in chain A are modeled at 85% occupancy and those associated with chain B are modeled at 100% occupancy. These values are consistent with the relative anomalous peak heights and individual occupancy refinement of the metal ions in PHENIX.[37] Minimal difference density in the $F_o - F_c$ map is observed near the Mn^{II} sites modeled using these occupancy values. Incomplete metal occupancy in chain A persists in crystals grown at higher pH (pH 7.0) or soaked in 10 mM $MnCl_2$ (Table S1 of the Supporting Information). Only cocrystallization of the protein in the presence of excess $MnCl_2$ (15 equiv) yielded full occupancy of all metal sites. Data collection statistics for the 15 equiv crystals are reported in Table 1 [*Bs* NrdF 15 equiv (Mn ano)]. The structure was determined by molecular replacement using the preliminary coordinates for *Bs* Mn^{II}_2-NrdF as the search model. Partial refinement of the structure was conducted as described above to determine metal occupancy, ligand conformations, and the presence of ordered solvent near the metal sites in each monomer.

Modeling of the *B. subtilis* NrdI−NrdF Complex and Solvent Channel. Solvent-accessible channels and cavities in *Bs* NrdF were calculated with HOLLOW using a 1.4 Å probe radius. *Bs* NrdI−NrdF model complexes were generated with the secondary structure matching superposition function in Coot[32] with the *Ec* $NrdI_{ox}$−NrdF complex (PDB entry 3N39)

dx.doi.org/10.1021/bi201925t | *Biochemistry* 2012, 51, 3861−3871

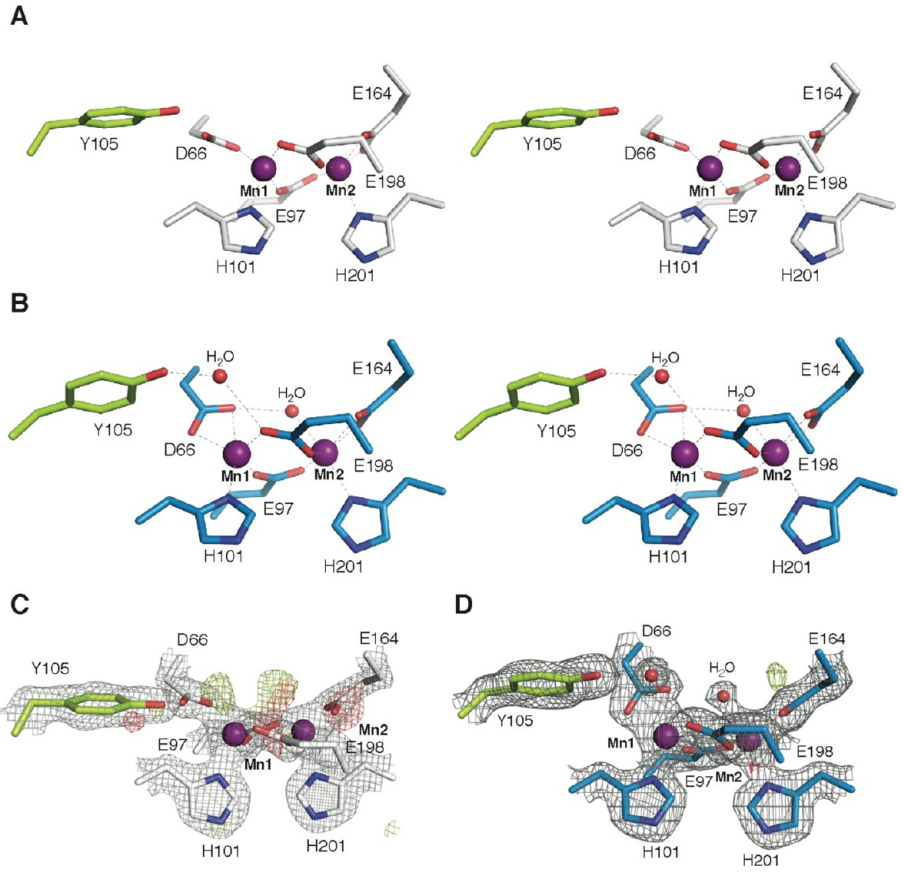

Figure 2. Stereoview of the metal sites [chain A (A) and chain B (B)] in *Bs* Mn^{II}_2-NrdF. The Mn ions are shown as purple spheres, and the coordinating amino acids and Tyr 105 (green) are represented as sticks and colored by atom type. Oxygen atoms associated with exogenous H_2O ligands are shown as red spheres. Mn−ligand bonds and hydrogen bonding interactions are shown as gray dashed lines. Active site electron density in *Bs* NrdF chain A (C) and chain B (D) with a $2F_o - F_c$ electron density map shown as gray mesh (1.5σ) and an $F_o - F_c$ map shown as green mesh (3.0σ) and red mesh (-3.0σ).

as the template and the X-ray structures of *Bs* $NrdI_{ox}$ (PDB entry 1RLJ) and *Bs* NrdF (this work) as query molecules. The *Ec* and *Bs* NrdF sequences are 44% identical, and the corresponding NrdI sequences are 31% identical. The *Bacillus cereus* NrdI−NrdF model was generated by the same method using a homology model of *B. cereus* NrdF (built using *Bs* NrdF, 60% identical, as the template) and the X-ray structure of the *B. cereus* semiquinone (sq) form of NrdI ($NrdI_{sq}$) (PDB entry 2X2P) as queries. The initial models yield few steric clashes at the interface. TRIAD (Protabit LLC) was used for the homology modeling and additional refinement of the complex models.

RESULTS

Overall Structure of *B. subtilis* Mn^{II}_2-NrdF. The 1.9 Å resolution X-ray structure of *Bs* Mn^{II}_2-NrdF (Table 1) was obtained by cocrystallizing N-terminally His_6-tagged apo NrdF (tag, MH_6SSGLVPRGSH) with 4 molar equiv of $MnCl_2$ (per $\beta 2$). This method of Mn^{II} loading has been used to generate Mn^{II}_2-NrdF for in vitro cofactor activation studies in solution[13,18] and to obtain the fully occupied structure of *Ec* Mn^{II}_2-NrdF.[21] The asymmetric unit for *Bs* Mn^{II}_2-NrdF contains two NrdF monomers arranged as a dimer in which the overall fold and quaternary structure are very similar to those of other class Ib $\beta 2$ proteins (Figure S1 of the Supporting Information).[14,21,24−26] Secondary structure matching superposition[38] with *Ec* Mn^{II}_2-NrdF, 44% identical in sequence, yields a root-mean-square deviation of 1.42 Å for 281 Cα atoms. Anomalous scattering data collected at the Mn absorption edge [6.65 keV (Table 1)] reveal the presence of Mn in the *Bs* NrdF metal sites (Figure S2 and Table S1 of the Supporting Information).

Structures of the Metal Sites. The structures of the Mn^{II}_2 clusters in chains A and B are shown in panels A and B of Figure 2, respectively, and schematically in panels A and B of Figure 3, respectively. Additionally, the electron density map for the Mn^{II}_2 site in each chain is shown in panels C and D of Figure 2. The Mn2 sites of the two chains are similar, but significant differences exist at Mn1. At the chain B metal site (Figures 2B and 3B), both Mn ions could be modeled at full occupancy with very little $F_o - F_c$ density near the first coordination sphere (Figure 2D and Figure S3 of the Supporting Information). The Mn ions are separated by 3.9 Å and bridged in a μ-1,3 fashion by residues Glu 97 and Glu 198. Mn2 is coordinatively saturated and additionally ligated by His 201 and Glu 164, the latter as a bidentate ligand. A weakly bound water molecule (Figures 2B and 3B) completes the first coordination sphere, in a position similar to that of the water in *Ec* Mn^{II}_2-NrdB[39] (Figure 1G). Mn1 is five-coordinate, bound to His 101 and Asp 66 in bidentate mode (Figures 2B and 3B). An ordered solvent molecule is also present near Mn1, within hydrogen bonding distance of Tyr 105, the site of stable $Y^{\bullet}$ formation in the active Mn^{III}_2-$Y^{\bullet}$ cofactor. This water molecule mediates the only hydrogen bonding interaction between Tyr

dx.doi.org/10.1021/bi201925t | *Biochemistry* 2012, 51, 3861−3871

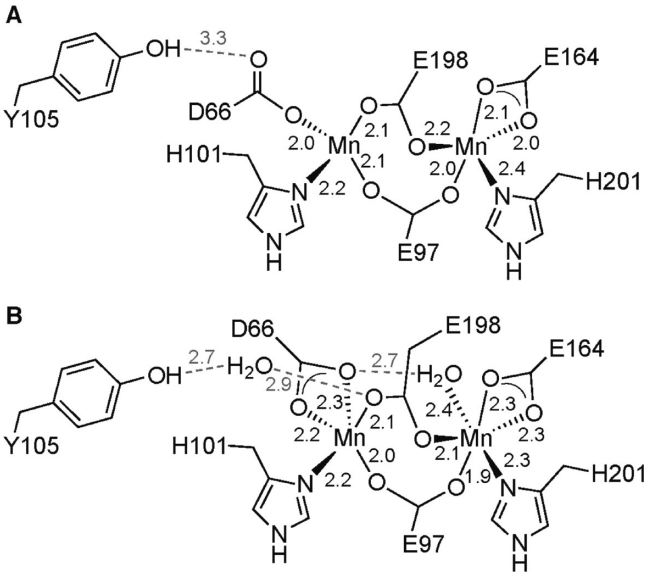

Figure 3. Schematic drawing of the active site configuration in chain A (A) and chain B (B) of *Bs* Mn^{II}_2-NrdF. Bond distances are given in angstroms, and hydrogen bonding interactions are illustrated as gray dashed lines.

105 and the Mn^{II}_2 active site, via Glu 198, bringing the tyrosine Oη atom within 5.7 Å of Mn1, similar to the corresponding distance in *Ec* Mn^{II}_2-NrdF (5.8 Å).[21] However, in the *Ec* case, Glu 192 (equivalent to Glu 198 of *Bs* NrdF) coordinates in a μ-η^1,η^2 fashion, creating space for the water molecule to be bound to Mn1, whereas this is sterically prohibited in *Bs* NrdF because of the μ-1,3 coordination of Glu 198.

The Mn^{II}_2 cluster in chain A (Figures 2A and 3A) is best modeled with 85% Mn occupancy in both sites, consistent with lower peak heights observed in the anomalous difference map (Table S1 and Figure S2 of the Supporting Information). Full occupancy of chain A can be achieved by cocrystallization with excess Mn^{II} (15 molar equiv/β2) (Table S1 and Figure S3C of the Supporting Information), but the coordination remains distinct from that of chain B. These observations are consistent with a lower Mn^{II} affinity and/or accessibility of the chain A metal site. Negative difference density near many of the ligands indicates some disorder in the first coordination sphere (Figure 2A and Figure S3A of the Supporting Information), and the presence of difference density even when crystals were grown with excess Mn^{II} (Figure S3C of the Supporting Information) indicates that the disorder at the metal site is not a result of incomplete Mn^{II} occupancy. Similar disorder is not observed in the fully occupied *Bs* NrdF chain B (Figure S3B of the Supporting Information) or *E. coli* Mn^{II}_2-NrdF[21] metal sites. As modeled, the ligand positions are similar to those of chain B. The exception is Asp 66, which in chain A adopts a monodentate coordination mode that allows it to interact directly with Tyr 105, as in *Ec* Mn^{II}_2-NrdF (Figure 1B) and reduced class Ia β2 structures.[23] Two areas of significant positive difference density (Figure 2C and Figure S3A of the Supporting Information) suggest that waters may be present in positions similar to those in chain B (Figure 2B and Figure S3B

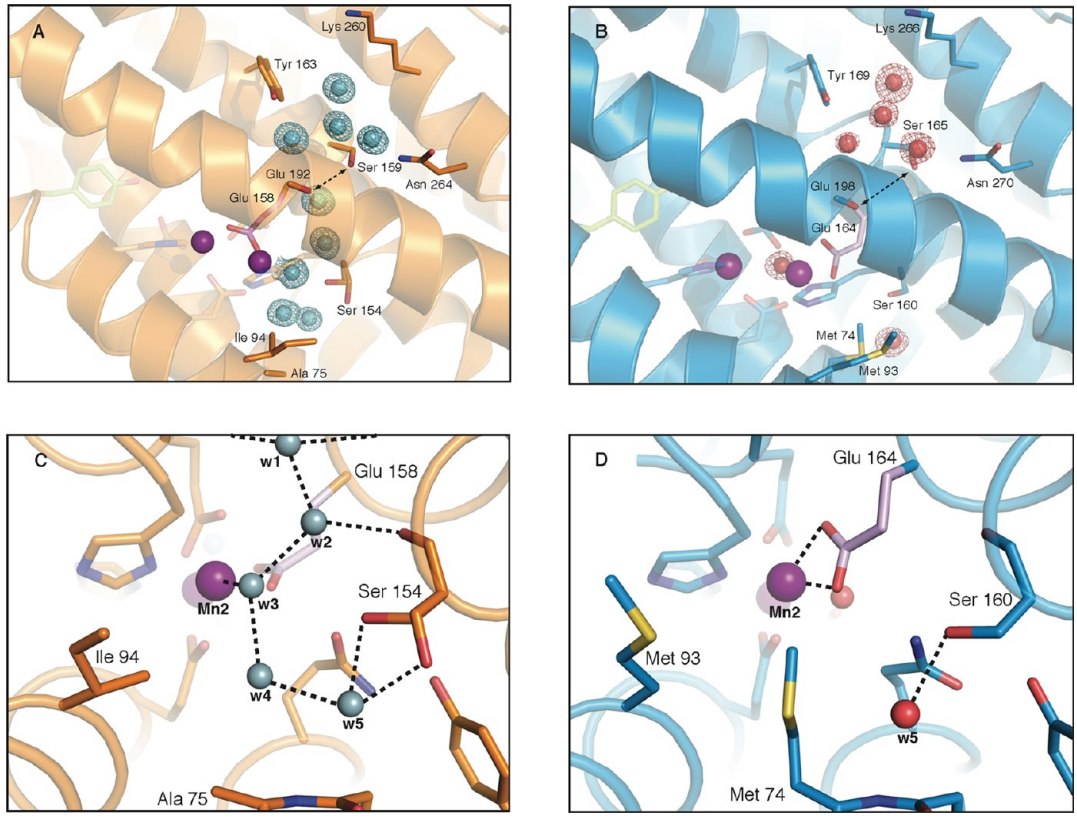

Figure 4. Solvent channel to Mn2 in the *Ec* (A) and *Bs* (B) Mn^{II}_2-NrdF structures. Residues lining the channel and active site residues are shown as sticks and colored by atom type. The active site ligand Glu 164/158 is colored pink, and the Mn ions are represented as purple spheres. A $2F_o - F_c$ electron density map showing ordered waters in the channels is shown as cyan (A, 1.5σ) or red (B, 1.2σ) mesh. (C and D) Enlarged views of the channel close to Mn2 in a slightly different orientation compared to panels A and B.

dx.doi.org/10.1021/bi201925t | *Biochemistry* 2012, 51, 3861−3871

of the Supporting Information). These were not modeled because of the absence of clear $2F_o - F_c$ electron density. In the data set obtained from *Bs* NrdF crystals grown with excess Mn^{II}, more $2F_o - F_c$ electron density is apparent, allowing a water molecule near Mn2 to be modeled (Figure S3C of the Supporting Information).

The overall structure of the metal site in chain A (and chain B, except for the ordered waters and the conformation of Asp 66) strongly resembles Fe^{II}_2-NrdFs from *E. coli*[21] (Figure 1A), *Salmonella typhimurium*,[25] and *Mycobacterium tuberculosis*.[26] However, the distance between Oη of Tyr 105 and Mn1 is 5.7 Å, ~1 Å shorter than in Fe^{II}_2-NrdF structures. This difference appears to be associated with a slight shift toward a bidentate coordination of Asp 66 in *Bs* chain A relative to *Ec* Fe^{II}_2-NrdF (the unbound Oδ is 3.1 Å from Mn1 as compared to 3.7 Å from Fe1 in *Ec* Fe^{II}_2-NrdF), preventing a water molecule from occupying the position between the Asp and Tyr as in *Ec* Fe^{II}_2-NrdF. A small difference in coordination of *Bs* NrdF Glu 97 (*syn*−*syn*) as compared to that of *Ec* Fe^{II}_2-NrdF Glu 98 (*syn*−*anti*) is also observed, perhaps related to the electron density suggesting water weakly bound to Mn2 (Figure 2C and Figure S3A,C of the Supporting Information) that is absent in *Ec* Fe^{II}_2-NrdF (Figure 1A).

Access of Solvent to the Metal Sites. All class Ib β2 structures exhibit a solvent-accessible channel near metal site 2 that opens at the surface of the protein[14,21,24−26] or, in the NrdI−NrdF complex, continues to the FMN cofactor of NrdI. This channel is proposed to be involved in access of the oxidant to the metal site. In *Ec* Mn^{II}_2-NrdF,[21] the μ-1,3 bridging mode of Glu 158 (Figure 1B, equivalent to *Bs* Glu 164) and coordination of a solvent molecule at Mn2 link site 2 directly to this channel (Figure 4A). Ala 75 and Ile 94 provide sufficient space for occupancy of the channel by waters in the crystal structure, forming a hydrogen-bonded network of ordered solvent near Mn2 [w1−w5 (Figure 4C)]. In *Bs* NrdF, Glu 164 is a bidentate ligand to Mn2, and Ala 75 and Ile 94 are replaced by methionines (Met 74 and Met 93), conserved in the Bacillales subclass of class Ib RNRs (Figure 4B and Figure S4 of the Supporting Information). The increased hydrophobicity and steric bulk of Met 74 effectively preclude ordered solvation of the oxidant channel in the vicinity of Mn2; only w5, within hydrogen bonding distance of Ser 160, and the water *trans* to His 201 are observed (Figure 4B,D).

The Mn1 coordination environment in *Bs* NrdF is also influenced by solvent (or lack thereof), and the degree of Mn1 solvent accessibility differs between chains A and B (Figure 5). This is related to a distinctive feature of the *Bs* Mn^{II}_2-NrdF structure involving the N-terminus of one β monomer in the asymmetric unit (Figure S1A of the Supporting Information). In all class Ia, Ib, and Ic β2 structures determined to date, the N-terminal tail of each chain interacts with the other chain of the dimer near metal site 1. In *Bs* NrdF chain B, residues 3−9 interact with chain A as in most other class I β2 structures (Figures S1A and S5A of the Supporting Information), and the density is continuous starting from Lys 3 (Figure S6A of the Supporting Information). This interaction is not observed for the N-terminus of *Bs* chain A. The first well-ordered residue in chain A is Trp 10, and little electron density (<1.5σ) is visible for residues 4−9 (Figure S6B of the Supporting Information). Although these residues have been modeled, their position is tentative because of the poor electron density. Stronger electron density that can be modeled as residues 1−3 forms a lattice contact with a symmetry-related molecule (Figure S5B−D of the Supporting Information).

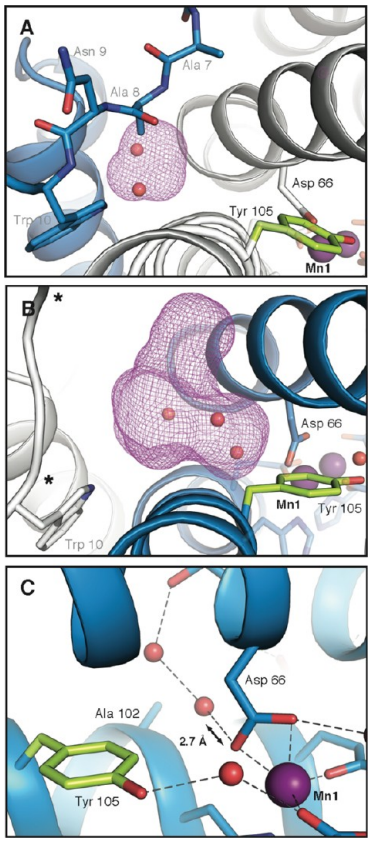

Figure 5. Bulk solvent access to Mn1 in *Bs* Mn^{II}_2-NrdF and the role of the N-terminus in the dimer interface. Pockets and channels that could accommodate solvent near site 1 are shown as purple mesh for chain A (A) and chain B (B). The open channel near Mn1 in chain B is occupied by two water molecules in the crystal structure, and a hydrogen bonding interaction between one of these waters and Asp 66 is possible (C). Residues involved in the channel are shown as sticks and colored by atom type and chain (chain A in white and chain B in blue). Residue Tyr 105 is colored green, and ordered waters are represented as red spheres. The disordered region spanning residues 3−10 in chain A is marked with asterisks.

In the *Bs* NrdF chain A metal site, a network anchored by residues 4−10 of the N-terminus of the adjacent chain B reduces solvent accessibility near Mn1 (Figure 5A), as in the other class I β2 structures.[14,21−26] In the chain B metal site, this network is disrupted by the disorder in the N-terminus of chain A (Figure 5B). Surprisingly, the disordered N-terminus in chain A correlates with higher metal occupancy and well-ordered electron density at the Mn^{II}_2 site in chain B. Additionally, a new solvent route to Mn1 appears, and two ordered water molecules are observed in a short channel linked to bulk solvent and terminating at one of the Oδ atoms of Asp 66 (Figure 5C). These waters may help enforce the observed bidentate coordination mode of Asp 66 (Figure 2B), allowing the second Oδ atom to move away from Tyr 105 and within hydrogen bonding distance of the solvent molecule associated with Mn2. Although the disorder in the C-terminus of chain A may be due to the crystallization conditions, the differences in coordination environment at each Mn^{II}_2 site illustrate how the individual positions of carboxylate and solvent ligands are tightly correlated in these types of active sites and further reveal that

dx.doi.org/10.1021/bi201925t | *Biochemistry* 2012, 51, 3861−3871

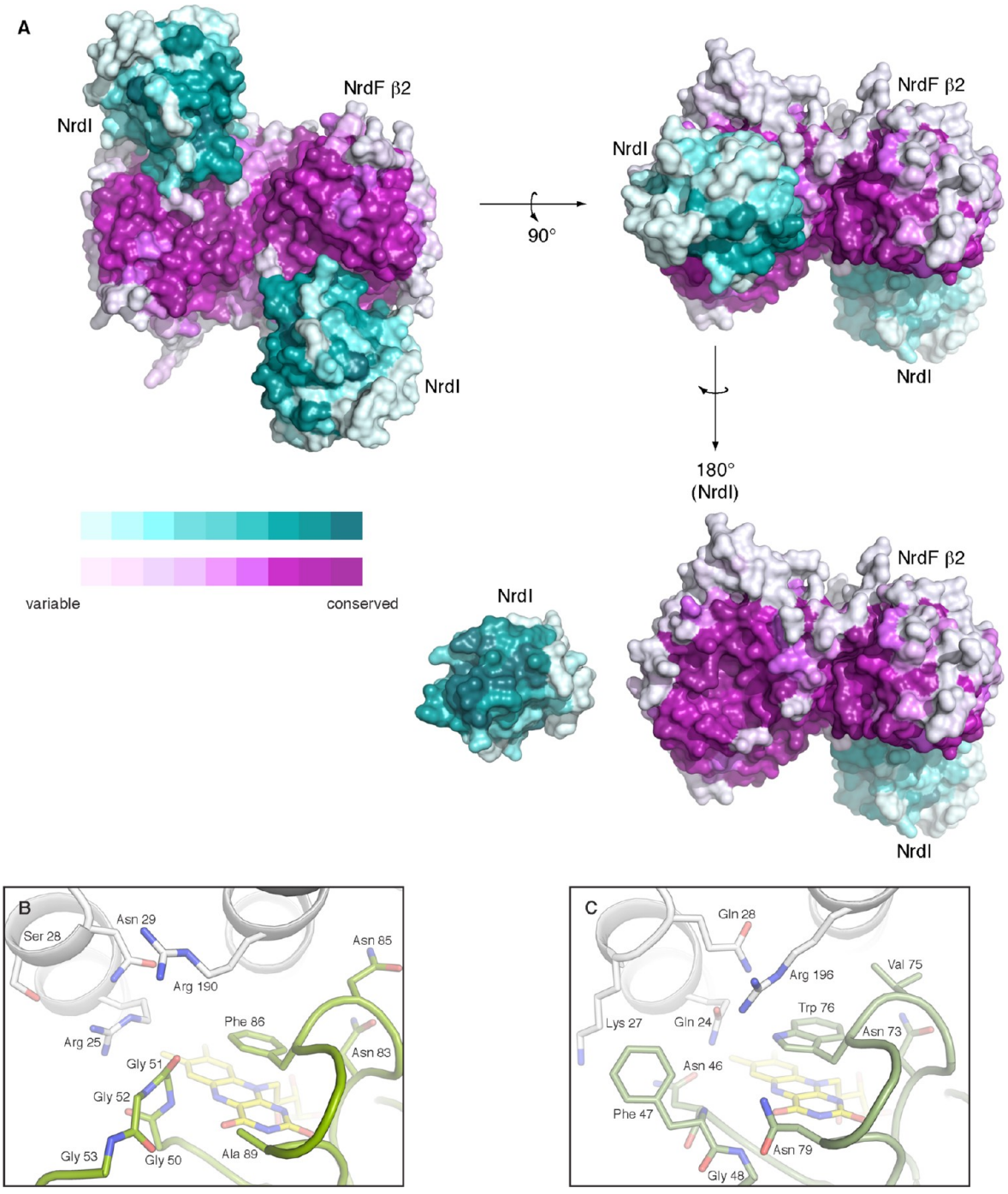

Figure 6. (A) Map of global sequence conservation (114 NrdF and 113 NrdI sequences[51]) in a superposition model of the *Bs* NrdI (PDB entry 1RLJ)−Mn^{II}_2-NrdF complex generated using the *Ec* NrdI−Mn^{II}_2-NrdF complex as a template. The top left view shows a conserved surface proposed to be involved in interaction with the α2 subunit. Rotation of the NrdI structure only (bottom right) shows the sequence conservation at the modeled interface. A cartoon and stick representation comparing the NrdI (green)−NrdF (white) interface in the vicinity of the NrdI FMN cofactor in the *Ec* $NrdI_{ox}$−Mn^{II}_2-NrdF crystal structure (PDB entry 3N39) (B) and the model of the *Bs* complex (C).

access to an extended solvent network can influence metal occupancy and the structure of the first coordination sphere.

Interface with NrdI. It is important to understand not only the structure of the NrdF metal site but also the interaction of *Bs* NrdI with NrdF, given that NrdI is required for Mn^{III}_2-$Y^{\bullet}$ cofactor assembly.[13,18] To gain insight into interaction surfaces of NrdI−NrdF pairs in general, 114 class Ib NrdF sequences were aligned and the extent of conservation was mapped onto the *Bs* NrdF structure (Figure 6A). These sequences represent three phylogenetically distinct groups:[3,40,41] actinobacterial and proteobacterial NrdFs (represented by *C. ammoniagenes* and *E. coli*, respectively), Bacillales NrdFs, primarily of the *Bacillus* and *Staphylococcus* genera (e.g., *B. subtilis*), and Lactobacillales NrdFs (no well-characterized examples to date). This analysis, shown in Figure 6A, reveals two clear regions with high levels of conservation on the surface of NrdF. The first region (Figure 6A, top left) is where the β2 subunit is presumed to interact with α2.[42,43] The second is the putative NrdI interface (Figure

dx.doi.org/10.1021/bi201925t | *Biochemistry* 2012, 51, 3861−3871

6A, bottom right). A model of *Bs* $NrdI_{ox}$ (PDB entry 1RLJ) complexed with *Bs* Mn^{II}_2-NrdF generated using the *Ec* $NrdI_{ox}$–NrdF structure[21] (Figure 6B) as a template is shown in Figure 6C. This complex was refined to eliminate the few steric clashes present in the initial model. Figure 6A shows significant sequence conservation at the putative interface, consistent with NrdI binding in the same general location on all NrdFs. It should be noted that analysis of available structures for NrdIs and NrdFs alone[14,21,24−26,41,44] and in complex[21] suggests that the NrdI–NrdF complex assembles in a preformed manner with little alteration of the protein fold in either component apart from rearrangement of side chains and peripheral loops.

Despite the sequence conservation, a closer look at the modeled interface predicts several prominent differences in the regions of NrdI and NrdF proximal to the NrdI FMN cofactor (Figure 6B,C). In particular, the composition and length of the loop ("50s loop" in *Ec* NrdI and "40s loop" in *Bs* NrdI) in the vicinity of the reactive C4a position of the FMN cofactor in NrdI are dramatically different. In *Bs* NrdI, the loop is three residues long with the NFG sequence, which is mostly conserved as (N/G)FG within this group. In *Ec* NrdI, the loop is seven residues long with a stretch of four consecutive glycine residues, a feature also largely conserved in its group. This loop makes important contacts with surface residues in *Ec* NrdF, particularly with a motif composed of Arg 190, Asn 29, and Arg 25 (Figure 6B). The 50s loop and some of the NrdF residues exhibit conformational changes dependent upon the redox state of the FMN cofactor of NrdI (Figure S7A,C of the Supporting Information).[21,41,44] The analogous surface in *Bs* NrdF differs significantly, substituting glutamine residues (conserved in Bacillales) for Asn 29 and Arg 25 (conserved in the *Ec* group) (Figure 6C). The FMN environment provided by the NrdI–NrdF complex is critical for the proposed roles of NrdI in NrdF cofactor assembly, production of the HOO(H) or $O_2^{\bullet-}$ oxidant by reaction of a reduced form of FMN with O_2, and channeling the oxidant through the NrdI–NrdF complex to the NrdF Mn^{II}_2 site.[13,21] The observed structural variations at the NrdI interface may therefore impact the cluster assembly mechanisms of the two class Ib RNR groups.

DISCUSSION

Comparison to Other Reduced Class I RNR Structures. The crystallographically characterized class I RNR β2 subunits substituted with Mn and Fe exhibit a diversity of dinuclear metal site configurations in their reduced forms (Figure 1). In the Fe^{II}-soaked structures of bacterial diferrous class Ib and Ia RNRs, the Fe1 and Fe2 sites are four- and five-coordinate, respectively, with no solvent ligands (Figure 1A,F).[21,23,24] This coordination environment is also observed in solution by circular dichroism (CD) and magnetic circular dichroism (MCD) studies of *E. coli* NrdB[45] and *B. cereus* NrdF.[46,47] The structure of *E. coli* Mn^{II}_2-NrdB, which cannot be activated in vitro or in vivo (Figure 1G), largely resembles the diferrous active sites,[21,23,24] but with a weakly bound water at Mn2 (2.4–2.5 Å Mn–O distance) *trans* to the His ligand. This latter structure is similar to the *Bs* Mn^{II}_2-NrdF structure presented here (Figures 1E and 2). Interestingly, in all of the available structures, Mn^{II} ions at both sites 1 and 2 support a higher coordination number than Fe^{II}. Only *Ca* Mn^{II}_2-NrdF (Figure 1C)[24] is an outlier, which may be the result of low metal occupancy and the presence of iron in the protein used for crystallization; for these reasons, this structure is not considered further. The coordination geometry observed in *Ec* Mn^{II}_2-NrdF[21] is quite distinct from the geometry of these other structures (Figure 1B). Although Mn2 is hexacoordinate, the location of its coordinated solvent molecule is not *trans* to the His ligand but instead to the oxygen atom of Glu 192 that bridges Mn1 and Mn2, and Glu 158 bridges the metal ions in a μ-1,3 mode rather than coordinating Mn2 alone (Figure 1). Thus, the *Bs* and *Ec* Mn^{II}_2-NrdF structures indicate that distinct reduced active site geometries can be the starting point for metallocofactor activation.

Access of Solvent to Mn2: Importance of the Secondary Coordination Sphere. Comparison of the *Bs* and *Ec* Mn^{II}_2-NrdF structures reveals that an important factor influencing the conformation of Glu 164/Glu 158 is the degree of access of solvent to Mn2 (Figure 4). In *Ec* Mn^{II}_2-NrdF, the oxidant channel is filled with contiguous ordered water molecules to Mn2, with two additional water molecules near Ala 75 and Ser 154.[21] The space for these solvent molecules past a constriction point in the channel at Ser 159 (Ser 165 in *B. subtilis*) is allowed by Ala 75 and Ile 94 and the μ-1,3 coordination of Glu 158. The Ala to Met substitution in *Bs* Mn^{II}_2-NrdF obviates water occupancy at the position of w4, which may be sufficient to disfavor formation of the w1–w3 network, and Glu 164 occupies the channel instead to coordinate Mn2 in the usual bidentate mode. With only two structures of Mn^{II}_2-NrdFs, it is difficult to assess which type of channel will be more common, although most non-Bacillales NrdF sequences have smaller residues (such as Ala 75 in *Ec* NrdF) at the position equivalent to *Bs* Met 74 (Figure S4 of the Supporting Information). Like *Bs* NrdF, *Ec* Fe^{II}_2-NrdF (despite the presence of Ala at position 75 instead of a Met) lacks ordered solvent between Ser 159 and metal site 2 and Glu 158 coordinates that site in bidentate fashion. However, in that case, the propensity of Fe^{II} for a coordination number lower than that of Mn^{II} in the class I RNR scaffold may be sufficient to exclude ordered water from the metal 2 site so that Glu 158 remains bidentate to Fe2 and the solvent channel cannot accommodate ordered water molecules below Ser 159. These observations highlight the interplay between protein side chains and solvent in the second coordination sphere in influencing the overall coordination geometry.

Implications for Access of the Oxidant to the Metal Site. As revealed by the crystal structure of the *Ec* NrdI–Mn^{II}_2-NrdF complex,[21] the proposed oxidant route in this class Ib system is traced by an extended network of water molecules that connects the flavin to Mn2 and is lined with hydrophilic amino acid residues. The sequence conservation map (Figure 6A) and our model of the *Bs* NrdI–NrdF complex (Figure 6C) indicate a high degree of sequence conservation of residues at the NrdI–NrdF interface, suggesting that *Bs* NrdI binds to *Bs* NrdF at a similar interface. Furthermore, 9 of the 10 amino acid residues lining the hydrophilic channel in the *Ec* NrdI–NrdF complex are completely conserved (the exception is the replacement of Asn 85 of *Ec* NrdI with Val 75 of *Bs* NrdI). The hydrophilic environment of the channel is augmented by backbone carbonyls of various residues, such as the extruded carbonyl of *Bs* Glu 164 and *Ec* Glu 158 in the π-helical segment of helix αE (Figure S8A,B of the Supporting Information). In all class Ib β2s, this π-helical distortion is stabilized by hydrogen bonds between carbonyl oxygens and solvent molecules (Figure S8A,B of the Supporting Information). By contrast, in class Ia *Ec* NrdB, the distortion is stabilized by a mechanism that does not involve solvent, a cation–π interaction involving a tyrosine (Tyr 209) and a conserved arginine (Arg 315), and the

carbonyl oxygen of the Glu 164 equivalent (Glu 204) is not involved in a hydrogen bond (Figure S8C of the Supporting Information). Furthermore, the presumed O_2 access channel in class Ia RNRs is formed by mostly hydrophobic residues that are also conserved. Thus, as we have suggested previously,[21] the degree of hydrophilicity of the respective putative oxidant channels in the class Ia and Ib RNRs appears to be well-correlated with the nature of the oxidants: nonpolar and hydrophobic O_2 for class Ia versus hydrophilic $O_2^{\bullet-}$ or HOO(H) for class Ib.

The *Bs* NrdF structure presented here and previous Fe^{II}_2-NrdF and Fe^{II}_2-NrdB structures suggest that the different oxidants used by class Ia and Ib RNRs to assemble their respective Fe^{III}_2-$Y^{\bullet}$ and Mn^{III}_2-$Y^{\bullet}$ cofactors may bind to metal site 2 in similar positions. For the initial step of assembly of Fe^{III}_2-$Y^{\bullet}$ from Fe^{II}_2-NrdB and O_2, the only existing structural insight is the crystal structure of the Phe208Ala/Tyr122Phe mutant of *Ec* NrdB soaked with azide.[48] The mutated residues are equivalent to *Bs* NrdF Phe 168, which forms a hydrophobic pocket directly over the metal site (Figure S8A of the Supporting Information), and Tyr 105. In this structure, the terminal nitrogen atom of the azide is 2.3 Å from Fe2, *trans* to the site 2 His ligand, at the position identical to that of the solvent molecule very weakly bound to Mn2 in the *Ec* Mn^{II}_2-NrdB structure (Figure 1G). Andersson et al. proposed that the azide-bound structure may represent an analogue to the structure of the diferrous site immediately upon O_2 binding.[49] By analogy, in Mn^{III}_2-$Y^{\bullet}$ assembly in *Bs* NrdF, we propose that the oxidant initially binds at Mn2, *trans* to His 201. Because all of the coordination positions on Mn2 are occupied, dissociation of the water molecule bound to Mn2 may gate access of the oxidant to the metal site.

Interface with NrdI. Biochemical and bioinformatics studies have also revealed significant differences between the *Ec* and *Bacillus* (*B. anthracis*, *B. cereus*, and *Bs*) systems in the properties of NrdI in relation to NrdF. These differences include the binding affinity of NrdI for NrdF,[13,18,50] the length of the 40s/50s loop in NrdI,[21,41,44] the electrostatic environment of the flavin in the NrdI−NrdF complex,[13,21,41] and the protonation state of the NrdI sq form stabilized in the presence of NrdF.[13] On the basis of these differences, some of the details of Mn^{III}_2-$Y^{\bullet}$ cofactor assembly are expected to be distinct in each group. We have previously noted that *Ec* NrdF Arg 25, which is positioned only 5−6 Å from the flavin N5 position (Figure 6B), may be an important factor in *Ec* NrdI's stabilization of the anionic form of its sq state in the presence of NrdF, whereas the flavin sq is neutral in the absence of NrdF.[13] Similar experiments involving *Bs* NrdI and NrdF show no evidence of anionic sq formation (unpublished data). A lower theoretical pI for the closely related *B. anthracis* and *B. cereus* NrdIs compared to that of *Ec* NrdI has been proposed to account for these differences,[41] but the protein surface closest to the FMN cofactor is similarly positive in all NrdIs. Additionally, the electrostatic environment of the NrdI FMN cofactor could be significantly influenced by interaction with NrdF. Comparison of the surface potentials for *Ec* and *Bs* NrdFs suggests that, while the surface of the protein where the flavin cofactor in NrdI would interact is similarly positive in both proteins, the proximity of Arg 25 in *Ec* NrdF may be specifically important in stabilizing the anionic sq in the *Ec* NrdI−NrdF complex. The position of this residue may in turn be regulated by hydrogen bonding interactions with the mobile 50s loop, the conformation of which is dependent on the redox state of the flavin. The equivalent residue in *Bs* NrdF, Gln 24, is situated in a position that should allow for hydrogen bonding interactions with the 40s loop of NrdI as well as with the indole NH group of Trp 76, which stacks above the flavin ring in NrdI (Figure 6C) and is conserved in the Bacillales group. Interestingly, the equivalent Trp residue adopts a different rotamer in the *B. anthracis* and *B. cereus* NrdIs,[41,44] which would preclude such an interaction. The position of the indole ring appears to correlate with the location of hydrophobic and polar residues in the vicinity of the flavin: in *B. subtilis*, the pyrrole portion of the indole would be positioned near Gln 24 of NrdF and Asn 79 of NrdI, and the benzene portion near Val 75 of NrdI; the corresponding residues in *B. anthracis* and *B. cereus* are Gln 20 of NrdF, Met 77 of NrdI, and Asn 73 of NrdI, respectively (Figure S7 of the Supporting Information). These observations underscore the importance of structural characterization of NrdI−NrdF complexes from several members of the *Bacillus* group.

Functional Significance of Metal Site Geometry in Class I RNRs. The differences in Glu 158/164 coordination, solvent occupation of the oxidant channel, and the influence of NrdF on the environment of the flavin in NrdI may indicate that *Ec* NrdF and *Bs* NrdF use different oxidant binding sites and possibly different oxidants. We previously proposed that the unique coordination geometry observed in the *Ec* Mn^{II}_2-NrdF structure reflects a distinct initial oxidant binding site for the class Ib NrdFs.[21] If *Ec* NrdF and *Bs* NrdF use the same oxidant, the significant structural differences exhibited by the two systems might reflect a situation in which some details of the reaction of O_2 with the flavin and conformational dynamics required to transport the oxidant to the metal site are different, rather than an entirely different mechanism of metal cluster oxidation. For example, a substantial conformational change would be needed to convert the metal site configuration observed in the *Ec* Mn^{II}_2-NrdF crystal structure, in particular the conformation of Glu 158, into one more similar to the *Bs* Mn^{II}_2-NrdF and other class I RNR structures. This model would suggest that the key distinction between the class Ia and Ib systems is not the structure of the metal site but rather the binding site for the specific accessory protein that provides an oxidant other than O_2 and the presence of a hydrophilic channel for that oxidant's access to the metal site. Further biochemical, crystallographic, and computational analyses of both systems are underway to test these hypotheses.

■ ASSOCIATED CONTENT

Ⓢ Supporting Information

Additional figures of the *Bs* NrdF structure. This material is available free of charge via the Internet at http://pubs.acs.org.

Accession Codes

The coordinates of *B. subtilis* Mn^{II}_2-NrdF have been deposited in the Protein Data Bank as entry 4DR0.

■ AUTHOR INFORMATION

Corresponding Author

*A.C.R.: telephone, (847) 467-5301; fax, (847) 467-6489; e-mail, amyr@northwestern.edu. J.S.: telephone, (617) 253-1814; fax, (617) 324-0505; e-mail, stubbe@mit.edu.

Funding

This work was supported by National Institutes of Health Grants GM58518 (A.C.R.) and GM81393 (J.S.), a National

Research Service Award fellowship to A.K.B., and a National Defense Science and Engineering Graduate fellowship to J.A.C.

Notes

The authors declare no competing financial interest.

■ ACKNOWLEDGMENTS

Use of the Advanced Photon Source, an Office of Science User Facility operated for the U.S. Department of Energy (DOE) Office of Science by Argonne National Laboratory, was supported by the U.S. DOE under Contract DE-AC02-06CH11357. Use of LS-CAT Sector 21 was supported by the Michigan Economic Development Corp. and the Michigan Technology Tri-Corridor (Grant 085P1000817). GM/CA CAT has been funded in whole or in part with Federal funds from the National Cancer Institute (Y1-CO-1020) and the National Institute of General Medical Sciences (Y1-GM-1104). We thank Benjamin Allen for technical assistance with generation and refinement of the *Bs* and *B. cereus* theoretical NrdI−NrdF models.

■ ABBREVIATIONS

β2, ribonucleotide reductase small subunit containing the metallocofactor; *Bs*, *B. subtilis*; *Ca*, *C. ammoniagenes*; CD, circular dichroism; *Ec*, *E. coli*; hq, FMN hydroquinone form; MCD, magnetic circular dichroism; ox, FMN oxidized form; PDB, Protein Data Bank; sq, FMN semiquinone form; RNR, ribonucleotide reductase; $Y^{\bullet}$, tyrosyl radical.

■ REFERENCES

(1) Nordlund, P., and Reichard, P. (2006) Ribonucleotide reductases. *Annu. Rev. Biochem. 75*, 681−706.

(2) Stubbe, J., Nocera, D. G., Yee, C. S., and Chang, M. C. (2003) Radical initiation in the class I ribonucleotide reductase: Long-range proton-coupled electron transfer? *Chem. Rev. 103*, 2167−2201.

(3) Cotruvo, J. A., Jr., and Stubbe, J. (2011) Class I ribonucleotide reductases: Metallocofactor assembly and repair in vitro and in vivo. *Annu. Rev. Biochem. 80*, 733−767.

(4) Solomon, E. I., Brunold, T. C., Davis, M. I., Kemsley, J. N., Lee, S. K., Lehnert, N., Neese, F., Skulan, A. J., Yang, Y. S., and Zhou, J. (2000) Geometric and electronic structure/function correlations in non-heme iron enzymes. *Chem. Rev. 100*, 235−349.

(5) Andrews, S. C. (2010) The ferritin-like superfamily: Evolution of the biological iron storeman from a rubrerythrin-like ancestor. *Biochim. Biophys. Acta 1800*, 691−705.

(6) Atkin, C. L., Thelander, L., Reichard, P., and Lang, G. (1973) Iron and free radical in ribonucleotide reductase. Exchange of iron and Mössbauer spectroscopy of the protein β2 subunit of the *Escherichia coli* enzyme. *J. Biol. Chem. 248*, 7464−7472.

(7) Jiang, W., Yun, D., Saleh, L., Barr, E. W., Xing, G., Hoffart, L. M., Maslak, M. A., Krebs, C., and Bollinger, J. M., Jr. (2007) A manganese(IV)/iron(III) cofactor in *Chlamydia trachomatis* ribonucleotide reductase. *Science 316*, 1188−1191.

(8) Jiang, W., Xie, J., Nørgaard, H., Bollinger, J. M., Jr., and Krebs, C. (2008) Rapid and quantitative activation of *Chlamydia trachomatis* ribonucleotide reductase by hydrogen peroxide. *Biochemistry 47*, 4477−4483.

(9) Stubbe, J., and Cotruvo, J. A., Jr. (2011) Control of metallation and active cofactor assembly in the class Ia and Ib ribonucleotide reductases: Diiron or dimanganese? *Curr. Opin. Chem. Biol. 15*, 284−290.

(10) Lundin, D., Torrents, E., Poole, A. M., and Sjöberg, B. M. (2009) RNRdb, a curated database of the universal enzyme family ribonucleotide reductase, reveals a high level of misannotation in sequences deposited to Genbank. *BMC Genomics 10*, 589.

(11) Jordan, A., Pontis, E., Atta, M., Krook, M., Gibert, I., Barbé, J., and Reichard, P. (1994) A second class I ribonucleotide reductase in Enterobacteriaceae: Characterization of the *Salmonella typhimurium* enzyme. *Proc. Natl. Acad. Sci. U.S.A. 91*, 12892−12896.

(12) Huque, Y., Fieschi, F., Torrents, E., Gibert, I., Eliasson, R., Reichard, P., Sahlin, M., and Sjöberg, B. M. (2000) The active form of the R2F protein of class Ib ribonucleotide reductase from *Corynebacterium ammoniagenes* is a diferric protein. *J. Biol. Chem. 275*, 25365−25371.

(13) Cotruvo, J. A., Jr., and Stubbe, J. (2010) An active dimanganese(III)-tyrosyl radical cofactor in *Escherichia coli* class Ib ribonucleotide reductase. *Biochemistry 49*, 1297−1309.

(14) Cox, N., Ogata, H., Stolle, P., Reijerse, E., Auling, G., and Lubitz, W. (2010) A tyrosyl-dimanganese coupled spin system is the native metalloradical cofactor of the R2F subunit of the ribonucleotide reductase of *Corynebacterium ammoniagenes*. *J. Am. Chem. Soc. 132*, 11197−11213.

(15) Stolle, P., Barckhausen, O., Oehlmann, W., Knobbe, N., Vogt, C., Pierik, A. J., Cox, N., Schmidt, P. P., Reijerse, E. J., Lubitz, W., and Auling, G. (2010) Homologous expression of the *nrdF* gene of *Corynebacterium ammoniagenes strain* ATCC 6872 generates a manganese-metallocofactor (R2F) and a stable tyrosyl radical ($Y^{\bullet}$) involved in ribonucleotide reduction. *FEBS J. 277*, 4849−4862.

(16) Cotruvo, J. A., Jr., and Stubbe, J. (2011) *Escherichia coli* class Ib ribonucleotide reductase contains a dimanganese(III)-tyrosyl radical cofactor in vivo. *Biochemistry 50*, 1672−1681.

(17) Martin, J. E., and Imlay, J. A. (2011) The alternative aerobic ribonucleotide reductase of *Escherichia coli*, NrdEF, is a manganese-dependent enzyme that enables cell replication during periods of iron starvation. *Mol. Microbiol. 80*, 319−334.

(18) Zhang, Y., and Stubbe, J. (2011) *Bacillus subtilis* class Ib ribonucleotide reductase is a dimanganese(III)-tyrosyl radical enzyme. *Biochemistry 50*, 5615−5623.

(19) Cotruvo, J. A., Jr., and Stubbe, J. (2008) NrdI, a flavodoxin involved in maintenance of the diferric-tyrosyl radical cofactor in *Escherichia coli* class Ib ribonucleotide reductase. *Proc. Natl. Acad. Sci. U.S.A. 105*, 14383−14388.

(20) Roca, I., Torrents, E., Sahlin, M., Gibert, I., and Sjöberg, B. M. (2008) NrdI essentiality for class Ib ribonucleotide reduction in *Streptococcus pyogenes*. *J. Bacteriol. 190*, 4849−4858.

(21) Boal, A. K., Cotruvo, J. A., Jr., Stubbe, J., and Rosenzweig, A. C. (2010) Structural basis for activation of class Ib ribonucleotide reductase. *Science 329*, 1526−1530.

(22) Strand, K. R., Karlsen, S., Kolberg, M., Røhr, A. K., Görbitz, C. H., and Andersson, K. K. (2004) Crystal structural studies of changes in the native dinuclear iron center of ribonucleotide reductase protein R2 from mouse. *J. Biol. Chem. 279*, 46794−46801.

(23) Voegtli, W. C., Sommerhalter, M., Saleh, L., Baldwin, J., Bollinger, J. M., Jr., and Rosenzweig, A. C. (2003) Variable coordination geometries at the diiron(II) active site of ribonucleotide reductase R2. *J. Am. Chem. Soc. 125*, 15822−15830.

(24) Högbom, M., Huque, Y., Sjöberg, B. M., and Nordlund, P. (2002) Crystal structure of the di-iron/radical protein of ribonucleotide reductase from *Corynebacterium ammoniagenes*. *Biochemistry 41*, 1381−1389.

(25) Eriksson, M., Jordan, A., and Eklund, H. (1998) Structure of *Salmonella typhimurium* NrdF ribonucleotide reductase in its oxidized and reduced forms. *Biochemistry 37*, 13359−13369.

(26) Uppsten, M., Davis, J., Rubin, H., and Uhlin, U. (2004) Crystal structure of the biologically active form of class Ib ribonucleotide reductase small subunit from *Mycobacterium tuberculosis*. *FEBS Lett. 569*, 117−122.

(27) Logan, D. T., Su, X. D., Aberg, A., Regnström, K., Hajdu, J., Eklund, H., and Nordlund, P. (1996) Crystal structure of reduced protein R2 of ribonucleotide reductase: The structural basis for oxygen activation at a dinuclear iron site. *Structure 4*, 1053−1064.

(28) Sazinsky, M. H., and Lippard, S. J. (2006) Correlating structure with function in bacterial multicomponent monooxygenases and related diiron proteins. *Acc. Chem. Res. 39*, 558−566.

(29) Rardin, R. L., Tolman, W. B., and Lippard, S. J. (1991) Monodentate carboxylate complexes and the carboxylate shift: Implications for polymetalloprotein structure and function. *New J. Chem. 15*, 417−430.
(30) Otwinowski, Z., and Minor, W. (1997) Processing of X-ray diffraction data collected in oscillation mode. *Methods Enzymol. 276*, 307−326.
(31) McCoy, A. J., Grosse-Kunstleve, R. W., Storoni, L. C., and Read, R. J. (2005) Likelihood-enhanced fast translation functions. *Acta Crystallogr. D61*, 458−464.
(32) Emsley, P., and Cowtan, K. (2004) Coot: Model-building tools for molecular graphics. *Acta Crystallogr. D60*, 2126−2132.
(33) Murshudov, G. N., Vagin, A. A., and Dodson, E. J. (1997) Refinement of macromolecular structures by the maximum-likelihood method. *Acta Crystallogr. D53*, 240−255.
(34) Laskowski, R. A. (1993) *PROCHECK*: A program to check the stereochemical quality of protein structures. *J. Appl. Crystallogr. 26*, 283−291.
(35) Chen, V. B., Arendall, W. B., III, Headd, J. J., Keedy, D. A., Immormino, R. M., Kapral, G. J., Murray, L. W., Richardson, J. S., and Richardson, D. C. (2010) MolProbity: All-atom structure validation for macromolecular crystallography. *Acta Crystallogr. D66*, 12−21.
(36) Delano, W. L. (2002) *The PyMOL molecular graphics system*, DeLano Scientific, San Carlos, CA.
(37) Zwart, P. H., Afonine, P. V., Grosse-Kunstleve, R. W., Hung, L. W., Ioerger, T. R., McCoy, A. J., McKee, E., Moriarty, N. W., Read, R. J., Sacchettini, J. C., Sauter, N. K., Storoni, L. C., Terwilliger, T. C., and Adams, P. D. (2008) Automated structure solution with the PHENIX suite. *Methods Mol. Biol. 426*, 419−435.
(38) Krissinel, E., and Henrick, K. (2004) Secondary-structure matching (SSM), a new tool for fast protein structure alignment in three dimensions. *Acta Crystallogr. D60*, 2256−2268.
(39) Atta, M., Nordlund, P., Aberg, A., Eklund, H., and Fontecave, M. (1992) Substitution of manganese for iron in ribonucleotide reductase from *Escherichia coli*. *J. Biol. Chem. 267*, 20682−20688.
(40) Torrents, E., Sahlin, M., Biglino, D., Gräslund, A., and Sjöberg, B. M. (2005) Efficient growth inhibition of *Bacillus anthracis* by knocking out the ribonucleotide reductase tyrosyl radical. *Proc. Natl. Acad. Sci. U.S.A. 102*, 17946−17951.
(41) Johansson, R., Torrents, E., Lundin, D., Sprenger, J., Sahlin, M., Sjöberg, B. M., and Logan, D. T. (2010) High-resolution crystal structures of the flavoprotein NrdI in oxidized and reduced states: An unusual flavodoxin. *FEBS J. 277*, 4265−4277.
(42) Uhlin, U., and Eklund, H. (1994) Structure of ribonucleotide reductase protein R1. *Nature 370*, 533−539.
(43) Uppsten, M., Farnegardh, M., Domkin, V., and Uhlin, U. (2006) The first holocomplex structure of ribonucleotide reductase gives new insight into its mechanism of action. *J. Mol. Biol. 359*, 365−377.
(44) Røhr, A. K., Hersleth, H. P., and Andersson, K. K. (2010) Tracking flavin conformations in protein crystal structures with Raman spectroscopy and QM/MM calculations. *Angew. Chem., Int. Ed. 49*, 2324−2327.
(45) Yang, Y. S., Baldwin, J., Ley, B. A., Bollinger, J. M., and Solomon, E. I. (2000) Spectroscopic and electronic structure description of the reduced binuclear non-heme iron active site in ribonucleotide reductase from *E. coli*: Comparison to reduced Δ^9 desaturase and electronic structure contributions to differences in O_2 reactivity. *J. Am. Chem. Soc. 122*, 8495−8510.
(46) Tomter, A. B., Bell, C. B., III, Røhr, A. K., Andersson, K. K., and Solomon, E. I. (2008) Circular dichroism and magnetic circular dichroism studies of the biferrous site of the class Ib ribonucleotide reductase from *Bacillus cereus*: Comparison to the class Ia enzymes. *Biochemistry 47*, 11300−11309.
(47) Other diferrous structures exist that were generated by chemical or photochemical reduction of a crystallized oxidized state.[25−27] These structures are not consistent with the CD and MCD data, and the water molecules present at their metal sites are likely derived from the μ-oxo-bridged diferric cluster.
(48) Andersson, M. E., Högbom, M., Rinaldo-Matthis, A., Andersson, K. K., Sjöberg, B. M., and Nordlund, P. (1999) The crystal structure of an azide complex of the diferrous R2 subunit of ribonucleotide reductase displays a novel carboxylate shift with important mechanistic implications for diiron-catalyzed oxygen activation. *J. Am. Chem. Soc. 121*, 2346−2352.
(49) Extrapolation of this structural information to O_2 binding is complicated by two factors. First, azide binding to the wild-type protein in the crystal was not observed; presumably, the Phe 208 to Ala mutation was required to prevent the Phe from sterically interfering with binding of the larger N_3^- (vs O_2) to the cluster. Second, the protein was crystallized in the Fe^{III}_2 form of the cluster, chemically reduced in the crystal, and soaked with azide; as mentioned previously, the crystal structures of chemically or photoreduced Fe^{III}_2-NrdB and Fe^{III}_2-NrdF are different from those of the apoprotein soaked with Fe^{II}.
(50) Crona, M., Torrents, E., Røhr, A. K., Hofer, A., Furrer, E., Tomter, A. B., Andersson, K. K., Sahlin, M., and Sjöberg, B. M. (2011) NrdH-redoxin mediates high enzyme activity in manganese-reconstituted ribonucleotide reductase from *Bacillus anthracis*. *J. Biol. Chem. 286*, 33053−33060.
(51) Landau, M., Mayrose, I., Rosenberg, Y., Glaser, F., Martz, E., Pupko, T., and Ben-Tal, N. (2005) ConSurf 2005: The projection of evolutionary conservation scores of residues on protein structures. *Nucleic Acids Res. 33*, W299−W302.